



Development and applications of Fe- and Co-based bulk glassy alloys and their prospects



A. Inoue^{a,b,d,*}, F.L. Kong^a, Q.K. Man^b, B.L. Shen^c, R.W. Li^b, F. Al-Marzouki^d

^a International Institute of Green Materials, Josai International University, Togane 283-8555, Japan

^b Ningbo Institute of Materials Technology & Engineering, Chinese Academy of Sciences, Ningbo 315201, China

^c School of Materials Science and Engineering, Southeast University, Nanjing 211189, China

^d Department of Physics, King Abdulaziz University, Jeddah 22254, Saudi Arabia

ARTICLE INFO

Article history:

Available online 27 November 2013

Keywords:

Bulk glassy alloys
Fe-based BMGs
Co-based BMGs
Applications

ABSTRACT

Glassy type metallic alloys exhibit unique characteristics which cannot be obtained for conventional amorphous alloys. For the last more than two decades, a number of bulk glassy alloy (BGA) systems have been developed and centimeter-class BGAs have been prepared in almost all alloy systems. Among them, Fe- and Co-based BGAs have attracted much attention and have been commercialized in various fields. This paper reviews recent developments and applications of Fe- and Co-based BGAs and their future prospects are also described.

© 2013 Elsevier B.V. All rights reserved.

1. Introduction

Around 1990, metallic glassy alloys in bulk form were found to be formed in La- and Mg-based systems by copper mold casting [1,2]. Subsequently, arc-melted Zr-based alloy ingots, just cooled on water-cooled copper hearth, were found to keep a glassy structure [3]. The ingot showed very shiny surface luster and had good ductility which could not be cracked by hitting with a hammer. Since the findings of these new phenomena, a great number of studies were carried out with the aims of searching new BGA systems, clarifying the fundamental properties including glass-forming ability (GFA), glassy structure and finding novel application fields [4–6]. As one of important results obtained for the last two decades, the lowest cooling rate for glass formation reaches 0.067 K/s, which is about 10^8 times smaller than that for ordinary amorphous alloys requiring melt quenching [7]. It is recognized that the thermal stability of supercooled liquid against crystallization increases dramatically and the enhanced stability has opened a new research field of metallic liquids. The maximum diameter (D_m) reaches about 8 cm for Pd–Cu–Ni–P system [8], 3 cm for Zr–Al–Ni–Cu [9,10], 5 cm for Zr–Ti–Be–Ni–Cu [11], 1.5–3 cm for Ni–Pd–P–B [12], and Cu–Zr–Al–Ag–Pd [13] and 7.3 cm for Cu–Zr–Al–Ag–Be [14]. In addition, glassy alloy plates with uniform thickness of 0.3–1 mm and large surface area aspect ratios have been produced as secondary forming materials [15]. Glassy alloy

balls with diameters of 2–10 mm are also available for the Zr- and Cu-based alloys [5].

The significant developments of BGAs have enabled the utilization of new bulk metallic materials consisting of a glassy structure since 1990, in addition to conventional bulk metallic crystalline materials which have been used by human beings for several thousand years. Table 1 summarizes the application fields that have been developed at present for glassy type alloys in Japan. The fields have been extended very widely.

Nowadays, sustainable developments have been desired to create low-carbon, resource-circulating and nature harmonious societies. We have been requested to contribute to sustainable development and low-carbon society through the developments of highly functional Fe- and Co-based BGAs and their industrialization. This review focuses on soft magnetic Fe- and Co-based alloys belonging to bulk glassy, nanocrystalline and bulk nanocrystalline types.

2. Fe-based bulk glassy alloys

2.1. Alloy components

Looking at the development history of Fe-based amorphous and glassy alloys, the first amorphous phase was synthesized for Fe–P–C system in 1967 by Paul Duwez's group [15], followed by the formation and licence of Fe- and Co-based amorphous alloys by Allied Chemical Corporation in 1975 [16] and their commercialization in the early 1980s. Subsequently, the synthesis of Fe-based BGAs by copper mold casting was made for Fe–Al–Ga–P–C–B alloys with a large supercooled liquid region before crystallization by Inoue et al. in 1995 [17].

Table 2 summarizes typical Fe-based BGAs developed up to date. The alloys can be classified to ferromagnetic and paramagnetic types at room temperature. As the former type, one can see Fe–(Al, Ga)–metalloid (P, C, B, Si) [17], Fe₂₀(Co–Si)–B

* Corresponding author at: International Institute of Green Materials, Josai International University, Togane 283-8555, Japan. Tel.: +81 475 53 2166.

E-mail address: ainouebmg@yahoo.co.jp (A. Inoue).

Table 1
Application fields for bulk glassy type alloys in Japan and their responding characteristic.

| Application fields | Characteristic |
|----------------------------------|---|
| Structural materials | High strength, high hardness, high fracture strength |
| Sensor materials | High magnetostriction, giant magneto-impedance effect |
| Spring materials | High fatigue strength |
| Sporting goods materials | High strength and large elastic elongation limit |
| Wear resistant coating materials | High wear resistance |
| Corrosion resistant materials | High corrosion resistance |
| Magnetic materials | Excellent soft-magnetic properties, high electrical resistivity |
| Micro-technology materials | Micro-formability, transferability |
| Nano-technology materials | Nanoscale imprintability |
| Data storage materials | |
| Biomedical materials | Biocompatibility, high wear and corrosion resistance |
| Fuel cell separator materials | |

Table 2
Typical Fe-based bulk glassy alloys developed up to date.

| Ferromagnetic alloys | Non-ferromagnetic alloys |
|-----------------------|--------------------------|
| Fe–(Al,Ga)–(P,C,B) | Fe–(Cr,Mo)–(C,B) |
| Fe–(P,Si)–(B,C) | (Fe,Ni)–(Cr,Mo)–(B,Si) |
| Fe–Ga–(P,C,B,Si) | Fe–(Cr,Mo)–(C,B)–Ln |
| Fe–(Cr,Mo)–(P,C,B,Si) | |
| Fe–(Zr,Hf,Nb)–B | |
| Fe–Co–Ln–B | |
| Fe–(Nb,Cr)–(B,Si) | |
| Fe–(Nb,Cr)–(P,B) | |
| Fe–(Zr,Hf,Nb)–B–Ln | |

(Fe-metalloid) [18,19], Fe–LTM(Cr, Mo)–metalloid [20], Fe–ETM(Zr, Hf, Nb)–metal-
loid [21], Fe–LTM–metalloid–(Y, Ln) (Ln = lanthanide metal) [22] and Fe–ETM–(B,
Si)–(Y, Ln) [23]. The latter type alloys are obtained for Fe–(Cr, Mo)–(C, B) [24],
(Fe, Ni)–(Cr, Mo)–(B, Si) [25] and Fe–(Cr, Mo)–(B, C)–(Y, Ln) [26–28].

These new Fe-based BGAs have been developed on the basis of the following
guidelines, i.e., (1) multicomponent systems consisting of three or more elements,
(2) significant atomic size mismatches among the main elements, (3) many atomic
pairs with negative heats of mixing and (4) minor addition of Al, Ga, ETM, LTM and
Y or Ln for enhancement of the three component rules.

2.2. Concrete results

2.2.1. Fe–(Ga, Mo)–(P, C, B, Si) alloy series

Glassy alloy rods of 2.5 mm in diameter are formed for $\text{Fe}_{77}\text{Ga}_3\text{P}_{9.5}\text{C}_4\text{B}_4\text{Si}_{2.5}$,
showing a supercooled temperature interval of 45 K, by copper mold casting [29].
The bulk GFA exhibits rather high saturation magnetization (B_s) of 1.4 T and low
coercive force (H_c) of 3 A/m. The replacement of Ga by Mo causes an increase of
 D_m to 4 mm for $\text{Fe}_{75}\text{Mo}_4\text{P}_{10}\text{C}_4\text{B}_4\text{Si}_3$ [30]. This alloy exhibits good combination
properties, i.e., 1.27 T for B_s , 1.5 A/m for H_c and 25,230 for effective permeability (μ_e) at
1 kHz and 1 A/m. By partial replacement of Fe with Co, the D_m increases further to
5 mm for $\text{Fe}_{66}\text{Co}_{10}\text{Mo}_{3.5}\text{P}_{10}\text{C}_4\text{B}_4\text{Si}_{2.5}$ [31], in conjunction with good soft magnetic
properties of 1.23 T for B_s , 1.0 A/m for H_c and 4.0×10^5 for maximum permeability
(μ_{max}) [31].

2.2.2. Fe–Co–Ni–B–Si–Nb alloy series

The addition of small amounts (2–4 at.%) of Nb to Fe–Si–B alloys was found to
cause the change from amorphous to glassy type with glass transition, followed by
supercooled liquid region over the whole composition range [32]. BGAs were
formed over the whole composition range of $[(\text{Fe}_{1-x-y}\text{Co}_x\text{Ni}_y)_{0.75}\text{B}_{0.2}\text{Si}_{0.05}]_{96}\text{Nb}_4$
and their D_m was 5 mm for $[(\text{Fe}_{0.5}\text{Co}_{0.5})_{75}\text{B}_{20}\text{Si}_{5}]_{96}\text{Nb}_4$ alloy [33]. The D_m for the
 $[(\text{Fe}_{0.5}\text{Co}_{0.5})_{75}\text{B}_{20}\text{Si}_{5}]_{96}\text{Nb}_4$ alloy increases to 7.7 mm by B_2O_3 flux melting [34].
The Fe-rich alloy exhibits rather high B_s of over 1.3 T [35], while the Co-rich alloy
has low H_c below 1 A/m because of very low saturated magnetostriction (λ_s) of
 5×10^{-7} under the field of 250 kA/m. The nearly zero λ_s alloy exhibits high μ_e
exceeding largely 10^4 in a wide frequency range up to at least 100 kHz, as exemplified
in Fig. 1 [36]. This good high-frequency permeability characteristic appears to
be maintained up to several MHz range.

2.2.3. Fe–Mo–Si–B–P alloy series

For $\text{Fe}_{76}\text{Si}_{9-x}\text{B}_{10}\text{P}_5\text{Mo}_x$ series, the D_m and B_s were, respectively, 3 mm and 1.45 T
for $x = 1$, 3.5 mm and 1.40 T for $x = 2$ [37]. Besides, the alloys with 1% and 2% Mo
show appreciable plastic strains in conjunction with fracture surface consisting of

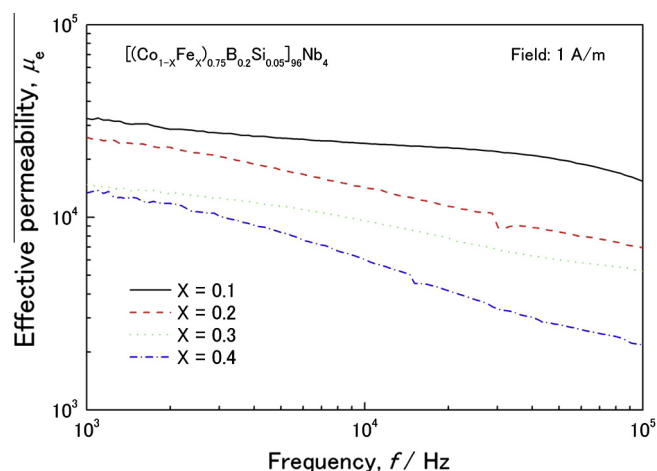


Fig. 1. Effective permeability as a function of applied field frequency for the
 $[(\text{Co}_{1-x}\text{Fe}_x)_{0.75}\text{B}_{0.2}\text{Si}_{0.05}]_{96}\text{Nb}_4$ ($x = 0.1, 0.2, 0.3,$ and 0.4) glassy alloys annealed for
300 s at temperature of $T_g - 50$ K.

several step zones. Even for the Mo-free Fe–Si–B–P alloys, BGAs were obtained in
the diameter range up to 2.5 mm and the $\text{Fe}_{79}\text{Si}_6\text{B}_{10}\text{P}_5$ alloy exhibits distinct plastic
strain of 1.1% [38]. The Fe–Si–B–P alloys exhibit very high B_s exceeding 1.6 T and the
maximum value reaches 1.62 T for $\text{Fe}_{80}\text{Si}_5\text{B}_{10}\text{P}_5$ [39]. The Fe–Si–B–P glassy alloys
also exhibit low H_c of 1.6–1.9 A/m and high μ_e of 16,500–17,200 at 1 kHz. It is no-
ticed that high B_s exceeding 1.6 T in conjunction with good soft magnetic properties
is obtained for Fe-metalloid alloy system.

2.2.4. Fe–Dy–B–Si–Nb alloy series

The influence of Ln addition on GFA, thermal stability and soft magnetic prop-
erties was examined for Fe–Dy–B–Si–Nb alloy series [40]. The 4%Dy-containing al-
loy shows a D_m of 4 mm and very large λ_s of 65×10^{-6} which are attractive for
application to a sensitive magnetostriction sensor.

3. Features of Fe-based bulk glassy alloys

Fe-based BGAs possess unique features of lower H_c and higher
electrical resistivity which have not been obtained for amorphous
and nanocrystalline Fe-based alloys [41]. The lower H_c has been
thought to originate from the lower internal stress on the basis
of the relation that H_c is dominated by some factors such as thick-
ness of domain wall, B_s , anisotropy constant and internal stress
[42]. With the aim of investigating the presumption, a number of
data for BGAs and amorphous alloys were re-plotted in the relation
between H_c and the ratio of λ_s to B_s [43]. In the relationship, the
data has a linear relation and its slope is much smaller for the BGAs
than for the amorphous alloys. The slope corresponds to the volume
and density of internal defects in the glassy and amorphous alloys.
The smaller slope implies that the BGAs include considerably lower

volume and density of defects, corresponding to the formation of more homogenized atomic configurations.

With the aim of confirming the structural presumption, we examined atomic configurations for Fe-based BGAs by using various advanced analytical techniques [44,45]. We have reported that Fe-based BGAs have a network-like atomic configuration in which distorted triangular and anti-Archimedean prisms are connected with each other with edge, face and vertices-shared configuration modes through glue atoms of rare earth or ETM element. Such a network-like atomic configuration can suppress the long-range atomic rearrangements of constituent elements which are necessary for the progress of crystallization. Consequently we can have highly stabilized supercooled liquid, leading to the formation of BGAs. For instance, the structure analyses on $\text{Fe}_{70}\text{Nb}_{10}\text{B}_{20}$ glassy alloy by synchrotron X-ray diffraction [46] and nanobeam electron diffraction [47] indicate the existence of edge-sharing distorted prism and anti-Archimedean prism. In addition, the primary crystallization phase of the $\text{Fe}_{70}\text{Nb}_{10}\text{B}_{20}$ alloy is composed of Fe_{23}B_6 type phase which has a complex cubic structure with a large unit volume of 1.0591^3 nm^3 and 116 atoms in unit cell and includes triangular and anti-Archimedean prisms [44]. The same type precipitation of M_{23}B_6 phase as a primary crystallization phase was also reported for $(\text{Fe}_{0.5}\text{Co}_{0.5})_{72}\text{B}_{20}\text{Si}_4\text{Nb}_4$ [48] and $\text{Fe}_{76}\text{Si}_7\text{B}_{10}\text{P}_5\text{Mo}_2$ [37] BGAs.

4. Fe- and Co-based bulk glassy alloys with centimeter class diameters

It is significant to investigate the relationship between the formations of Fe- and Co-based BGAs and their crystallization phases. Fig. 2 shows the change in the D_m with Co content for $(\text{Fe}_{1-x}\text{Co}_x)_{48}\text{Cr}_{15}\text{Mo}_{14}\text{C}_{15}\text{B}_6\text{TM}_2$ alloys prepared by casting, together with the X-ray diffraction data [49]. The D_m is 12 mm for the Fe–Cr–Mo–C–B–Tm alloy, increases to 16 mm in the Co range of 0.2–0.4 and then decreases to 10 mm for the Co–Cr–Mo–C–B–Tm alloy. We further recognized that the more fine adjustment of alloy component to $(\text{Fe}_{0.8}\text{Co}_{0.2})_{47}\text{Cr}_{15}\text{Mo}_{14}\text{C}_{15}\text{B}_6\text{TM}_3$ caused the further increase of D_m to 18 mm [41].

Fig. 3 shows the DSC curves of the Fe–Cr–Mo–C–B–Tm BGAs in as-cast bulk and melt-spun ribbon forms, together with the electron diffraction patterns of the alloys annealed at each temperature marked with arrows [44]. The glassy alloy crystallizes through two stages and the first exothermic peak appears from the supercooled liquid region. The electron diffraction pattern obtained after annealing for 30 min at 973 K is identified as a complex cubic Fe_{23}B_6 phase, indicating that the second peak corresponds to the precipitation of Fe_{23}B_6 phase [44].

On the other hand, one cannot detect any appreciable change in the electron diffraction patterns after annealing around the first exothermic peak. Further detailed nanobeam analyses were carried out to clarify the precipitation phase due to the first peak. As shown in Fig. 4 [44], the nanobeam diffraction pattern is identified as cubic χ -FeCrMo phase with rather large unit volume of 8.92^3 nm^3 and 58 atoms in unit cell. The atom number in χ -FeCrMo phase is just half that for Fe_{23}B_6 phase and the fundamental unit is composed of a CN16 polyhedron structure for the former phase and a CN16 polyhedron surrounding the central Archimedean antiprism including large amounts of metalloid atoms for the latter phase [48], indicating a strong correlation between the two phases. From the DSC curves and nanobeam electron diffraction patterns, it is concluded that the two-stage crystallization occurs through the primary precipitation of χ -FeCrMo phase and then the precipitation of Fe_{23}B_6 phase [44].

It has been further reported that Fourier transformation pattern obtained from the atomic configurations in χ -FeCrMo phase shows

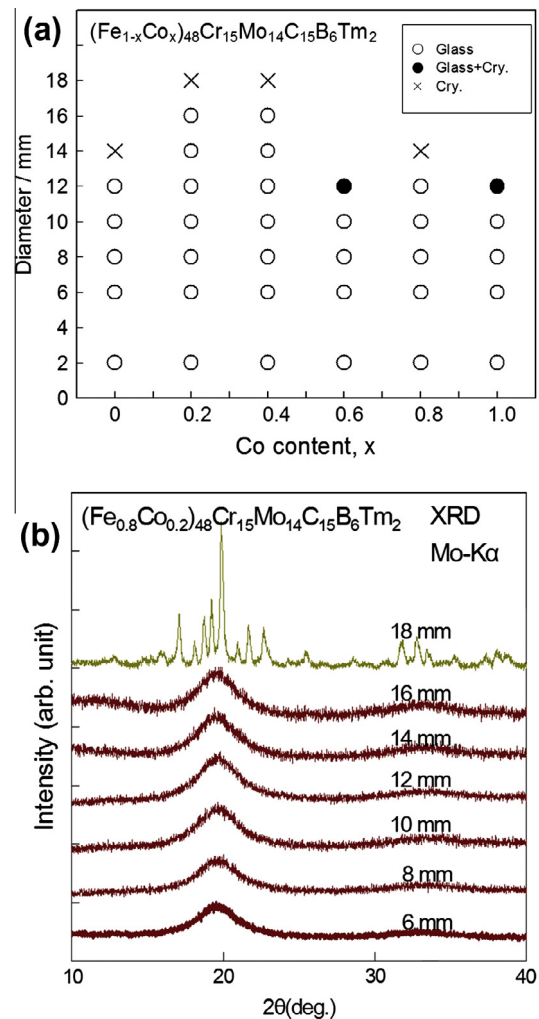


Fig. 2. (a) Change in the structure of the cast $(\text{Fe}_{1-x}\text{Co}_x)_{48}\text{Cr}_{15}\text{Mo}_{14}\text{C}_{15}\text{B}_6\text{TM}_2$ rods with sample diameter and Co content. (b) X-ray diffraction data of $(\text{Fe}_{0.8}\text{Co}_{0.2})_{48}\text{Cr}_{15}\text{Mo}_{14}\text{C}_{15}\text{B}_6\text{TM}_2$ rods with different diameters.

the electron diffraction patterns with a ten-fold symmetry [50]. This result suggests that the Fe-based BGAs with centimeter class diameters are composed of icosahedral-like atomic configurations and hence the unique atomic configurations may play an important role in the achievement of the large GFA. Thus, we can propose the searching way of Fe-based BGAs with centimeter class diameters through the alloy design of forming icosahedral atomic configurations.

5. Fe-based bulk glassy alloys as structural materials

In 2000, we reported that the addition of a small amount (1.5 at.%) of B to commercial FC20 alloy ($\text{Fe}_{80.75}\text{C}_{13.8}\text{Si}_{5.1}\text{Mn}_{0.18}\text{P}_{0.15}\text{S}_{0.02}$) enabled the formation of glassy alloy rod with a diameter of about 0.5 mm by copper mold casting [18]. The glassy alloy exhibited high tensile fracture strength of 3480 MPa and increased to 3850 MPa upon annealing for 15 min at 680 K. Even after crystallization to bcc-Fe and $\text{Fe}_3(\text{C},\text{B})$ phases, the alloy rod exhibits high yield strength of about 1250 MPa as well as large tensile elongation exceeding 10%. In addition, the alloy rod can be bent to an almost circular ring-shape after annealing for 15 min at 1200 K. These good mechanical properties for the FC20 alloy containing 1.5%B are promising for structural Fe-based materials because of the features of inexpensiveness alloy and simple production way.

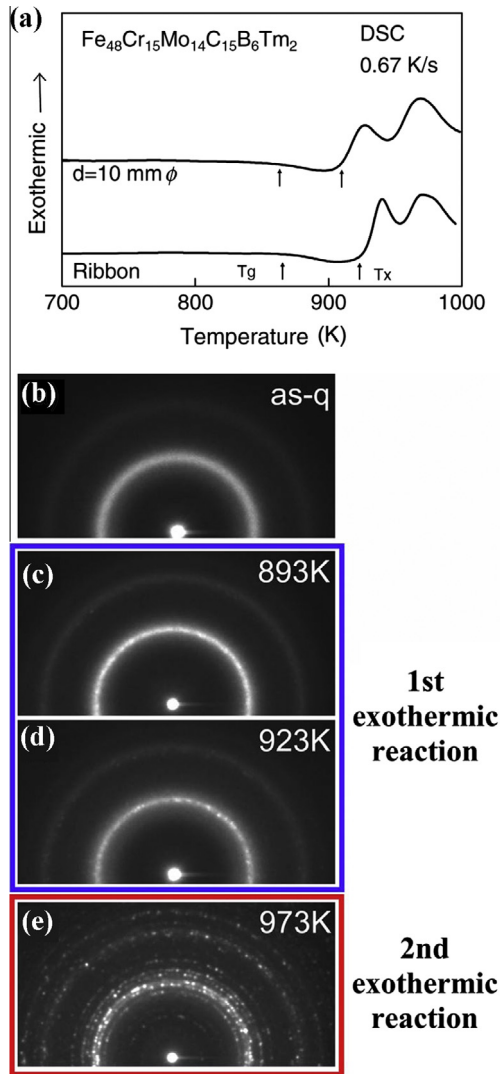


Fig. 3. (a) DSC curves obtained from $\text{Fe}_{48}\text{Cr}_{15}\text{Mo}_{14}\text{C}_{15}\text{B}_6\text{Tm}_2$ ribbon and bulk specimens. Energy-filtered SAED patterns obtained from (b) as-quenched specimen and specimens annealed at (c) 893, (d) 923, and (e) 973 K. The diameter of the selected area is approximately 400 nm.

As another interesting data indicating the possibility as structural materials, BGAs with diameters up to 2.5 mm are formed by casting and the addition of trace amounts (0.1–0.5 at.%) of Cu enables the formation of glassy alloys containing nanoclusters [51]. The BGAs including nanoclusters exhibit distinct compressive ductility with plastic strains up to 4% and numerous shear bands are observed on the lateral outer surface.

6. Fe-based nanocrystalline alloys with ribbon form

It is known that nanocrystalline Fe-based soft magnetic alloys have been commercialized with trademarks of FINEMET [52] and NANOPERM [53]. The former consists of Fe–Si–B–Nb–Cu and the latter is composed of Fe–Zr–B–Cu. Based on the developments of their nanocrystalline alloys, the development guideline has been proposed [54]. When the size of bcc grains in Fe-based nanocrystalline alloys is smaller than the exchange length, the magnetocrystalline anisotropy is averaged out by coupling mechanism between bcc nanograins through the remaining ferromagnetic amorphous phase. In addition, the nanocrystalline alloys show

nearly zero λ_s . Therefore, the alloys are expected to exhibit excellent soft magnetic properties.

For Fe–Si–B–P amorphous alloys with two-stage crystallization mode, Cui et al. examined the change in the crystallization mode with Cu addition [55]. By the addition of 0.7–1.0% Cu, the first exothermic peak shifts to low temperature side, while the second peak remains almost unchanged, resulting in an extension of the temperature interval between the two peaks. When the sample is annealed at the temperature below the second exothermic peak, fine bcc grains with 20 nm in size precipitate in the Fe–Si–B–P–Cu alloys. The bcc grains are surrounded by the remaining amorphous phase and their intergranular spacing is evaluated to be about 1 nm by high-resolution TEM observation [56]. The three dimensional atom probe (3DAP) analyses indicate that the intergranular amorphous phase is enriched with B and P, while the bcc phase has higher Si and Cu concentrations than the nominal compositions. The distinct component segregation after annealing seems to cause the high stability of nanoscale bcc gains.

Table 3 summarizes the grain size of bcc-Fe phase (D), magnetization at 800 A/m (B_{800}), B_s , H_c , μ_e at 1 kHz and λ_s of Fe–Si–B–P–Cu [57,58] and Fe–Si–B–C–Cu [59] nanocrystalline alloys, together with the previous data of other soft magnetic materials, i.e., FINEMET [52], NANOPERM [53], Fe–Si steels [60] and amorphous alloy (METGLAS 2605) [56]. The new nanocrystalline alloys in Fe–Si–B–P–Cu and Fe–Si–B–Cu systems have unique features, i.e., simultaneous achievement of high B_s and high permeability which has not been obtained for other soft magnetic alloys. The new nanocrystalline alloys exhibit lower core losses in the high magnetic induction range of 1.5–1.7 T [57,61], as compared with FINEMET, oriented Fe–Si steels and amorphous alloys. It is therefore concluded that the step wise improvement of core loss characteristics will be able to reduce energy consumption as well as carbon dioxide gas emission.

7. Fe-based nanocrystalline bulk alloys

Glassy $\text{Fe}_{73-x}\text{Nb}_4\text{Hf}_3\text{Y}_x\text{B}_{20}$ alloys prepared by casting exhibited distinct glass transition, followed by supercooled liquid region and then crystallization [62]. The D_m and the temperature interval of supercooled liquid region are, respectively, 1.5 mm and 63 K for the 0%Y alloy, 3 mm and 75 K for the 1%Y alloy, and 4 mm and 78 K for the 2%Y alloy.

When the 0%Y alloy is annealed for 180 s at 885 K, the XRD pattern reveals that the alloy consists of bcc-Fe and remaining amorphous phase and the grain size of the bcc-Fe phase is about 20 nm [63]. The nanocrystalline alloy exhibits high B_s of about 1.5 T. It is believed that this is the first evidence for the formation of Fe-based nanocrystalline alloys exhibiting simultaneously bulk GFA, high B_s of 1.5 T, glass transition and rather wide supercooled liquid region where viscous flow deformation is possible.

8. Relation between glass-forming ability and χ -FeCrMo phase for Fe-based bulk glassy alloys

Here it is important to describe that the GFA increases by the addition of Y and Co elements. The D_m increases to 4 mm for $\text{Fe}_{71}\text{Nb}_4\text{Hf}_3\text{Y}_2\text{B}_{20}$ alloy, 6 mm for $(\text{Fe}_{0.7}\text{Co}_{0.3})_{71}\text{Nb}_4\text{Hf}_3\text{Y}_2\text{B}_{20}$ and 7 mm for $(\text{Fe}_{0.6}\text{Co}_{0.4})_{71}\text{Nb}_4\text{Hf}_3\text{Y}_4\text{B}_{20}$ [63]. Fig. 5 shows the DSC curves of $(\text{Fe}_{0.6}\text{Co}_{0.4})_{71}\text{Nb}_4\text{Hf}_3\text{Y}_4\text{B}_{20}$ glassy alloy, together with the X-ray diffraction data. The alloy exhibits the glass transition with a wide supercooled liquid region of 95 K and a small exothermic peak in the supercooled liquid region. The X-ray diffraction patterns indicate that the primary precipitation is M_{23}B_6 phase [63].

Considering that the primary precipitation phase for Fe–Cr–Mo–C–B–Tm alloys with centimeter class diameters is χ -FeCrMo

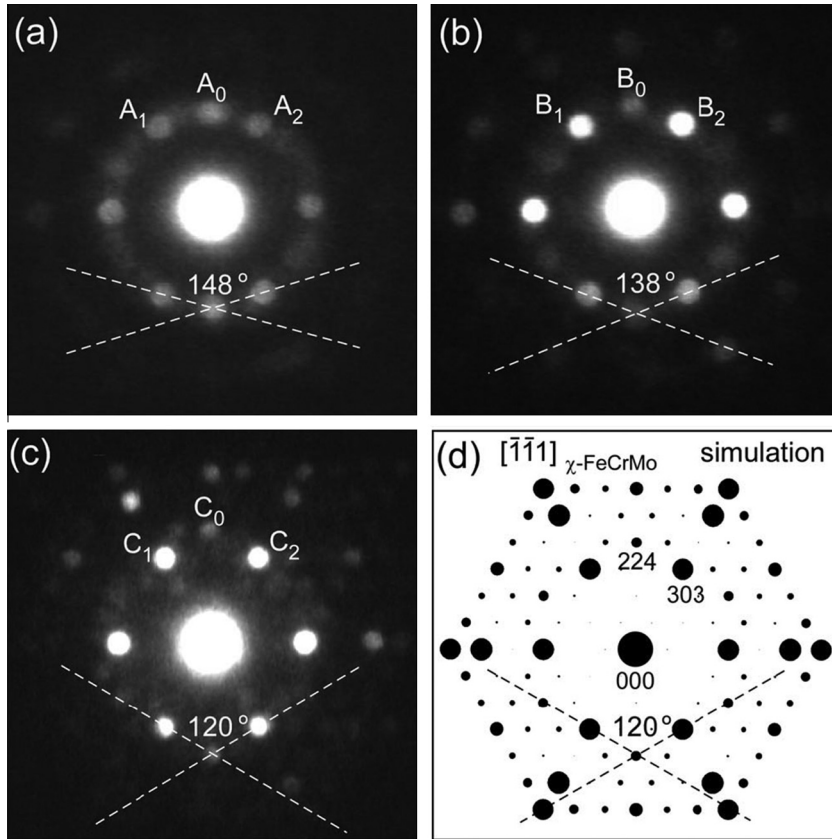


Fig. 4. NBED patterns captured from the specimens annealed at [(a) and (b) 893 K and (c) 923 K along with a simulated diffraction pattern of χ -FeCrMo. The electron incidence of pattern (d) is parallel to the $[\bar{1}\bar{1}1]_{\chi\text{-FeCrMo}}$ direction. Pattern (c) is consistent with the simulated pattern, whereas patterns (a) and (b) are slightly different. The angles among three diffraction spots denoted by A_1 – A_0 – A_2 , B_1 – B_0 – B_2 , and C_1 – C_0 – C_2 are also shown in the figures.

Table 3

The grain size of bcc-Fe phase (D), magnetization at 800 A/m (B_{800}), saturated magnetization (B_s), coercive force (H_c), effective permeability at 1 kHz (μ_e) and saturated magnetostriction (λ_s) of Fe–Si–B–P–Cu and Fe–Si–B–C–Cu nanocrystalline alloys.

| Materials (at.%) | D (nm) | B_{800} (T) | B_s (T) | H_c (A/m) | μ_e (1 kHz) | λ_s (10^{-6}) |
|--|----------|---------------|-----------|-------------|-----------------|---------------------------|
| Fe ₈₅ Si ₂ B ₈ P ₄ Cu ₁ | 16 | 1.82 | – | 5.8 | 27,000 | 2.3 |
| Fe ₈₆ Si ₁ B ₈ P ₄ Cu ₁ | 19 | 1.85 | – | 2.8 | 24,000 | 2.4 |
| Fe _{82.65} Si ₂ B ₉ P ₅ Cu _{1.35} | 15 | – | 1.80 | 1.1 | 37,000 | – |
| Fe _{83.3} Si ₄ B ₈ P ₄ Cu _{0.7} | 10 | – | 1.88 | 7 | 25,000 | 2 |
| Fe _{84.3} Si ₄ B ₈ P ₄ Cu _{0.7} | 17 | – | 1.94 | 10 | 16,000 | 3 |
| Fe ₈₃ B ₁₀ C ₄ Si ₂ Cu ₁ | 15 | – | 1.78 | 4 | 13,600 | – |
| Fe _{73.5} Si _{13.5} B ₉ Nb ₃ Cu ₁ | 20 | 1.23 | 1.24 | 0.5 | 150,000 | 2.1 |
| Fe ₉₀ Zr ₇ B ₃ | 13 | – | 1.7 | 5.8 | 30,000 | –1.1 |
| Fe ₇₈ Si ₉ B ₁₃ | – | 1.49 | – | 2.6 | 10,600 | 27 |
| Fe–6.5 mass% Si | – | – | 1.85 | 45 | 31,000 | 6.8 |

[44], the small exothermic peak for the Fe–Co–Nb–Hf–Y–B alloy with D_m of 7 nm may be due to the precipitation of χ -FeCrMo including icosahedral-like atomic configuration, though the X-ray diffraction pattern was identified as $M_{23}B_6$ due to the similarity between $M_{23}B_6$ and χ -FeCrMo phases. The further detailed analyses on this point by using advanced analytical techniques are under investigation.

Table 4 summarizes the relationship among alloy component, D_m , crystallization mode and the first crystallization phase for typical Fe-based BGAs. One can notice some features, (1) the necessity of Y or Ln to form a centimeter class BGA, (2) the appearance of small exothermic peak in the supercooled liquid region, resulting in multi-stage crystallization mode, (3) systematic change in the primary precipitation phase from $M_{23}B_6$ to χ -FeCrMo through the addition of Y or Ln, and (4) the centimeter class BGAs always have the primary precipitation mode of χ -FeCrMo phase having

icosahedral-like atomic configuration. It is thus confirmed that the formation of BGAs with centimeter class diameters is due to the development of the unique atomic configuration. It is also important to clarify the reason why the addition of Y or Ln causes the development of icosahedral-like atomic configuration for Fe-based multi-component alloys, though the addition enhances the level of satisfaction of the three component rules for formation of BGAs.

9. Applications of Fe-based bulk glassy alloys

It has been shown in this review that Fe-based BGAs exhibit simultaneously high GFA, low H_c , high μ_m and μ_e , high electrical resistivity, low core losses, high mechanical strength, large elastic strain and large supercooled liquid region leading to viscous flow deformation, though the B_s is less than 1.5 T. Here, it is important

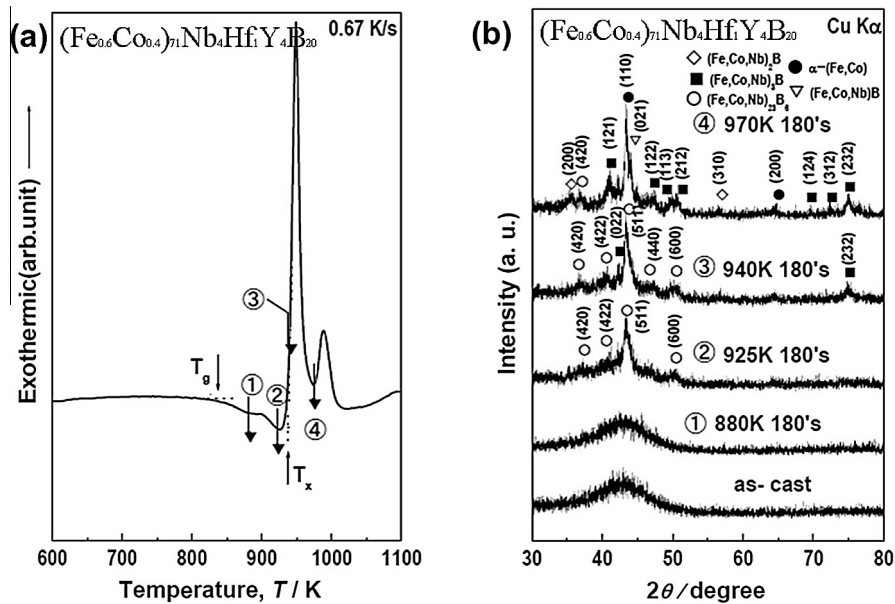


Fig. 5. (a) DSC curves and (b) X-ray diffraction patterns of $(\text{Fe}_{0.6}\text{Co}_{0.4})_{71}\text{Nb}_4\text{Hf}_1\text{Y}_4\text{B}_{20}$ glassy alloys in as-cast and annealed states.

to describe that the high GFA for Fe-based alloys enables the production of glassy alloy powders over a wide powder size range even by cheap mass production technique such as water atomization. By utilizing these advantages, some Fe-based BGAs have already been commercialized with trademarks of “Liquialloy” [64], “SENNTIX” [65], “GALOA” [66], “AMO-beads” [67], etc. When we focus on the application of soft magnetic Fe-based alloys, the examples of “Liquialloy” and “SENNTIX” are presented in this section.

The “Liquialloy” has been produced by simple processes of mass production of glassy alloy powders, followed by mixing the powders with resin, cold consolidation and then annealing at low temperatures. Through the simple production process, ALPS Co. has developed compact low core loss conversion inductors [68]. The inductors have been used in DC/DC converters in notebook PCs and servers as well as point of load power supplies. Another example is the development of compact high precision power sensing devices with excellent temperature stability, i.e., compact power control current sensors. “Liquialloy” has also been used as high efficient and large current type power inductors in CPU and graphics power supply circuits for notebook PCs, DC/DC converters for servers, game consoles and point of load power supplies.

Liquialloy powders can be deformed to a flaky shape with a thickness of 2–3 μm and large aspect ratios of 20–30. By mixing the flaky powders with resin, Liquialloy sheet can be produced. The sheet can efficiently convert electromagnetic noise to heat

and hence suppress the noise. The sheet has been commercialized as noise suppression sheet in various electromagnetic instruments [68]. Furthermore, the sheet has been used as radio frequency identification (RFID) system. The insertion of Liquialloy sheet between metal device part and loop antenna is able to increase transmission distance of magnetic flux line to the inside of loop antenna, resulting in a significant increase of antenna sensitivity at a carrier frequency of 13.56 MHz. By utilizing these advantages, the RFID system using Liquialloy sheet has been used in cell phones such as NTT DoCoMo FOMA type.

Another type of soft magnetic alloy in Fe–P–B–Nb–Cr system with trademark of SENNTIX II has been developed through collaboration study between Tohoku University and NEC/TOKIN Corporation [69]. The advantages of SENNTIX II are high GFA and much lower H_c as compared with Fe–Si–B amorphous alloys. The use of consolidated SENNTIX choke coil is able to reduce more than 50% core loss from existing metal power and save thermal losses at PC board, resulting in an extension of battery life time of notebook PC by about 10%. Therefore, the SENNTIX choke coil has been commercialized since 2009.

10. Co-based bulk glassy alloys

It has already been presented that Co-based ferromagnetic BGAs exhibit many features; (1) low H_c , (2) high μ_m and μ_e , (3)

Table 4

The relationship among alloy component, maximum diameter for glass formation, crystallization mode and the first crystallization phase for typical Fe-based bulk glassy alloys.

| Alloy component | Maximum diameter (mm) | Crystallization mode | First crystallization phase |
|--------------------------|-----------------------|----------------------|---|
| Fe–(C,B)–(P,Si) | 1–3 | Single stage | α -Fe |
| Fe–(C,B)–(P,Si)–(Cr,Mo) | 5 | Single stage | $(\text{Fe, Mo})_{23}(\text{B, C})_6$ |
| (Fe,Co)–B–Si–Nb | 5.5 | Single stage | $(\text{Fe, Co})_{23}(\text{B, Nb})_6$ |
| (Fe,Co)–(C,B)–(P,Si)–Mo | 5 | Single stage | $(\text{Fe, Co, Mo})_{23}(\text{C, B})_6$ |
| Fe–B–Mo–Y | 6.5 | Multi-stage | $(\text{Fe, Mo})_{23}\text{B}_6$ |
| (Fe,Co)–B–(Nb,Hf)–Y | 7 | Multi-stage | $(\text{Fe, Co, Nb})_{23}\text{B}_6$ |
| Fe–(C,B)–(Cr,Mo)–Tm | 12 | Multi-stage | χ -FeCrMo |
| Co–(C,B)–(Cr,Mo)–Tm | 10 | Multi-stage | χ -FeCrMo |
| (Fe,Co)–(C,B)–(Cr,Mo)–Tm | 18 | Multi-stage | χ -FeCrMo |

nearly zero λ_s , (4) low high-frequency loss, (5) low λ_s coefficient leading to Giant Magneto-Impedance (GMI) effect, (6) high fracture strength exceeding 4000 MPa, (7) high glass transition and crystallization temperatures, (8) large supercooled liquid region, (9) high corrosion resistance, and (10) high wear resistance, etc. However, the D_m of Co-based ferromagnetic glassy alloys is about 2 mm for $(\text{Co}_{0.705}\text{Fe}_{0.045}\text{B}_{0.25-x}\text{Si}_x)_{96}\text{Nb}_4$ [70], though paramagnetic Co-based alloys are obtained for the rod diameter of 10 mm [49].

Recently, the fine adjustment of alloy components has increased the D_m to 4.5 mm for $\text{Co}_{46}\text{Fe}_{20}\text{B}_{23}\text{Si}_5\text{Nb}_6$ [71] and 5.5 mm for $(\text{Co}_{0.7}\text{Fe}_{0.3})_{68}\text{B}_{21.9}\text{Si}_{5.1}\text{Nb}_5$ [72]. These Co-based BGAs also exhibit good characteristics. Their B_s , H_c , μ_e and fracture strength are 0.63–0.69 T, 1.2–2.4 A/m, 13,600–26,500 and 4400 MPa, respectively, for the former alloy, and 0.49–0.91 T, 0.71–1.58 A/m, 22,100–32,500 and 4250–4450 MPa, respectively, for the latter.

It is noticed that the $(\text{Co}_{0.6}\text{Fe}_{0.4})_{64}\text{B}_{21.9}\text{Si}_{5.1}\text{Nb}_5$ BGA exhibits distinct plastic strain with serrated flow [72]. The D_m of the nearly zero λ_s alloy also increases by fine adjustment of alloy component and reaches 4 mm for $(\text{Co}_{0.942}\text{Fe}_{0.058})_{67}\text{Nb}_5\text{B}_{22.4}\text{Si}_{5.6}$ [73]. The alloy exhibits good combination properties, i.e., 3600 MPa for fracture strength, 0.43 T for B_s , 0.2 A/m for H_c and 47165 for μ_e at 1 kHz and 1 A/m.

Furthermore, the addition of lanthanide element (Er, Tb, Y or Dy) enables a significant increase of supercooled liquid region and the largest interval reaches 130 K for $(\text{Co}_{0.5}\text{Fe}_{0.5})_{62}\text{Nb}_6\text{Dy}_2\text{B}_{30}$ [74]. In the supercooled liquid region, the alloy exhibits good superplastic formability as well as excellent nanoscale imprintability.

Owing to the above advantage points, Co-based BGAs have been tested for commercialization to position sensor, antenna for radio-controlled watch, solenoid valve and magnetic sensor, etc. For instance, the magnetic sensors using Co–Fe-based BGAs have been confirmed to exhibit sharper transient signal, higher output voltage and higher mechanical strength. However, real commercialization has not been achieved for Co-based BGAs because of their high materials cost, in contrast to the real commercialization state for Fe-based BGAs.

11. Conclusion

Over the past two decades, Fe- and Co-based BGAs have been developed for various applications and significant progress has been made. However, great efforts are still need to further reduce the costs and improve the combination properties as well as reliability through future improvements of alloy designing and production technique. It is expected that the new engineering material will be able to contribute to the future progress of sustainable society and low-carbon society.

References

- [1] A. Inoue, T. Zhang, T. Masumoto, Mater. Trans. JIM 31 (1990) 425–428.
- [2] A. Inoue, A. Kato, T. Zhang, S.G. Kim, T. Masumoto, Mater. Trans. JIM 32 (1991) 609–616.
- [3] T. Zhang, A. Inoue, T. Masumoto, Unpublished Research, Tohoku University (1990).
- [4] A. Inoue, Acta Mater. 48 (2000) 279–306.
- [5] W.L. Johnson, MRS Bull. 24 (1999) 42–56.
- [6] A. Inoue, A. Takeuchi, Acta Mater. 59 (2011) 2243–2267.
- [7] N. Nishiyama, A. Inoue, Appl. Phys. Lett. 80 (2002) 568–570.
- [8] N. Nishiyama, K. Takenaka, H. Miura, N. Saidoh, Y. Zeng, A. Inoue, Intermetallics 30 (2012) 19–24.
- [9] A. Inoue, T. Zhang, Mater. Trans. JIM 37 (1996) 185–187.
- [10] Y. Yokoyama, E. Mund, A. Inoue, L. Schultz, Mater. Trans. 48 (2007) 3190–3192.
- [11] W.L. Johnson, Mater. Sci. Forum 35 (1996) 225–227.
- [12] Z. Yuqiao, N. Nishiyama, A. Inoue, Mater. Trans. 50 (2009) 1243–1246.
- [13] Q. Zhang, W. Zhang, A. Inoue, Mater. Trans. 48 (2007) 3031–3033.
- [14] H. Lou, X. Wang, F. Xu, S. Ding, Q. Cao, K. Hono, J. Jiang, Appl. Phys. Lett. 99 (2011) 051910.
- [15] P. Duwez, S.C.H. Lin, J. Appl. Phys. 38 (1967) 4096–4097.
- [16] H.S. Chen, Rep. Prog. Phys. 43 (1980) 353–432.
- [17] A. Inoue, Y. Shinohara, J.S. Gook, Mater. Trans. JIM 36 (1995) 1427–1433.
- [18] A. Inoue, X.M. Wang, Acta Mater. 48 (2000) 1383–1395.
- [19] A. Makino, T. Kubota, M. Makabe, C.T. Chang, A. Inoue, Mater. Sci. Eng., B 148 (2008) 166–170.
- [20] S. Pang, T. Zhang, K. Asami, A. Inoue, Mater. Trans. JIM 42 (2001) 376–379.
- [21] A. Inoue, T. Zhang, A. Takeuchi, Appl. Phys. Lett. 71 (1997) 464–466.
- [22] A. Inoue, B.L. Shen, AIP Conf. Proc. 832 (2006) 11–20.
- [23] A. Inoue, H. Kimura, B.L. Shen, J. Metastable Nanocryst. Mater. 20 (2004) 3–12.
- [24] S. Pang, T. Zhang, K. Asami, A. Inoue, Acta Mater. 50 (2002) 489–497.
- [25] K. Okumura, J. Kurosaki, K. Nishimura, S. Kimura, A. Inoue, Mater. Japan 43 (2004) 142–144 (in Japanese).
- [26] V. Ponnambalam, S.J. Poon, G.J. Shiflet, J. Mater. Res. 19 (2004) 1320–1323.
- [27] Z.P. Lu, C.T. Liu, J.R. Thompson, W.D. Porter, Phys. Rev. Lett. 92 (2004) 245503.
- [28] K. Amiya, A. Inoue, Rev. Adv. Mater. Sci. 18 (2008) 27–29.
- [29] B.L. Shen, A. Inoue, Mater. Trans. 43 (2002) 1235–1239.
- [30] B.L. Shen, M. Akiba, Appl. Phys. Lett. 88 (2006) 131907.
- [31] M.X. Zhang, F.L. Kong, A.D. Wang, C.T. Chang, B.L. Shen, J. Appl. Phys. 111 (2012) 07A312.
- [32] A. Inoue, B.L. Shen, Mater. Trans. 43 (2002) 766–769.
- [33] A. Inoue, B.L. Shen, C.T. Chang, Acta Mater. 52 (2004) 4093–4099.
- [34] T. Bitoh, A. Makino, A. Inoue, A.L. Greer, Appl. Phys. Lett. 88 (2006) 182510.
- [35] A. Inoue, B.L. Shen, A. Takeuchi, Mater. Trans. 47 (2006) 1275–1285.
- [36] B.L. Shen, C.T. Chang, T. Kubota, A. Inoue, J. Appl. Phys. 100 (2006) 013515.
- [37] J. Zhang, B.L. Shen, Z. Zhang, J. Non-Cryst. Solids 360 (2013) 31–35.
- [38] A. Makino, T. Kubota, C.T. Chang, M. Makabe, A. Inoue, J. Magn. Magn. Mater. 320 (2008) 2499–2503.
- [39] J. Zhang, C.T. Chang, A. Wang, B.L. Shen, J. Non-Cryst. Solids 358 (2012) 1443–1446.
- [40] J. Li, H. Men, B.L. Shen, AIP Adv. 1 (2011) 042110.
- [41] C. Suryanarayana, A. Inoue, Int. Mater. Rev. 58 (2013) 131–166.
- [42] T. Bitoh, A. Makino, A. Inoue, Mater. Trans. 44 (2003) 2020–2024.
- [43] T. Bitoh, A. Makino, A. Inoue, J. Appl. Phys. 99 (2006) 08F102.
- [44] A. Hirata, Y. Hirotsu, K. Amiya, A. Inoue, Phys. Rev. B 78 (2008) 144205.
- [45] A. Hirata, Y. Hirotsu, K. Amiya, N. Nishiyama, A. Inoue, Phys. Rev. B 80 (2009) 140201.
- [46] T. Hanada, Y. Hirotsu, T. Ohkubo, Mater. Trans. 45 (2004) 1194–1198.
- [47] A. Hirata, Y. Hirotsu, E. Matsubara, Mater. Trans. 46 (2005) 2781–2784.
- [48] A. Hirata, Y. Hirotsu, K. Amiya, N. Nishiyama, A. Inoue, Mater. Sci. Forum 539–543 (2007) 2077–2081.
- [49] K. Amiya, A. Inoue, Mater. Trans. 47 (2006) 1615–1618.
- [50] A. Hirata, Y. Hirotsu, K. Amiya, A. Inoue, J. Alloys Comp. 504 (2010) S186–S189.
- [51] A. Makino, X. Li, K. Yubuta, C. Chang, T. Kubota, A. Inoue, Scr. Mater. 60 (2009) 277–280.
- [52] Y. Yoshizawa, S. Oguma, K. Yamauchi, J. Appl. Phys. 64 (1988) 6044–6046.
- [53] K. Suzuki, A. Makino, N. Kataoka, A. Inoue, T. Masumoto, Mater. Trans. JIM 32 (1991) 93–102.
- [54] G. Herzer, IEEE Trans. Magn. 26 (1990) 1397–1402.
- [55] L. Cui, H. Men, A. Makino, T. Kubota, K. Yubuta, M. Qi, A. Inoue, Mater. Trans. 50 (2009) 2515–2520.
- [56] A. Makino, T. Kubota, K. Yubuta, A. Inoue, A. Urata, H. Matsumoto, S. Yoshida, J. Appl. Phys. 109 (2011) 07A302–305.
- [57] A. Makino, T. Kubota, K. Yubuta, A. Inoue, A. Urata, H. Matsumoto, S. Yoshida, J. Appl. Phys. 109 (2011) 07A302.
- [58] F.L. Kong, H. Men, T.C. Liu, B.L. Shen, J. Appl. Phys. 111 (2012) 07A311.
- [59] X.D. Fan, H. Men, A.B. MA, B.L. Shen, Sci. China, Ser. E 55 (2012) 2416–2419.
- [60] M. Abe, Y. Takada, T. Murakami, Y. Tanaka, Y. Mihara, J. Mater. Eng. 11 (1989) 109–116.
- [61] A. Makino, H. Men, T. Kubota, K. Yubuta, A. Inoue, Mater. Trans. 50 (2009) 204–209.
- [62] Z. Long, Y. Shao, F. Xu, H. Wei, Z. Zhang, P. Zhang, X. Su, Mater. Sci. Eng., B 164 (2009) 1–5.
- [63] Y. Shao, Preparation and properties of Fe-group based metallic glassy alloys, Doctor Thesis, Tohoku University, 2008.
- [64] H. Koshiba, Y. Naito, T. Mizushima, A. Inoue, Mater. Japan 47 (2008) 39–41 (in Japanese).
- [65] H. Matsumoto, A. Urata, Y. Yamada, A. Inoue, IEEE Trans. Magn. 46 (2010) 373–376.
- [66] A. Inoue, H. Kimura, M. Ohara, I. Takanori, Japan Patent, JP 2006–214000.
- [67] K. Okumura, J. Kajita, J. Kurosaki, H. Kimura, A. Inoue, in: Abstr. in 10th int'l conf. on shot peening, Tokyo, Japan, September 15–18, 2008.
- [68] D.V. Louzguine-Luzgin, A. Inoue, Handbook of Magnetic Materials, Elsevier, 2013.
- [69] H. Matsumoto, A. Urata, Y. Yamada, A. Inoue, J. Alloys Comp. 504 (2010) S139–S141.
- [70] B.L. Shen, Y. Zhou, C.T. Chang, A. Inoue, J. Appl. Phys. 101 (2007) 09N101.
- [71] Q.K. Man, H.J. Sun, Y.Q. Dong, B.L. Shen, H. Kimura, A. Makino, A. Inoue, Intermetallics 18 (2010) 1876–1879.
- [72] Y.Q. Dong, A.D. Wang, Q.K. Man, B.L. Shen, Intermetallics 23 (2012) 63–67.
- [73] H.J. Sun, Q.K. Man, Y.Q. Dong, B.L. Shen, H. Kimura, A. Makino, A. Inoue, J. Alloys Comp. 504 (2010) S31–S33.
- [74] Q.K. Man, A. Inoue, Y.Q. Dong, J. Qiang, C.L. Zhao, B.L. Shen, Scr. Mater. 69 (2013) 553–556.